

Approximate Quantum Compiling for Quantum Simulation: A Tensor Network based approach

Niall F. Robertson¹, Albert Akhriev¹, Jiri Vala^{2,3} and Sergiy Zhuk¹

¹ IBM Quantum, IBM Research Europe - Dublin, IBM Technology Campus, Dublin 15, Ireland

² Maynooth University, Maynooth, Ireland

³ Tyndall National Institute, Cork, Ireland

Abstract

The simulation of quantum spin chains is a promising candidate for the demonstration of quantum advantage. One of the main obstacles to achieving this is the noise that arises from implementing the deep circuits that appear in standard quantum time evolution algorithms. Compiling these deep circuits into shallower ones is thus a key issue that we address in this work. We use a Tensor Network based approach to Approximate Quantum Compiling to produce short depth quantum circuits that simulate the time evolution of the Heisenberg spin chain on up to 100 qubits. Furthermore, we run these short depth circuits on a *ibmq-mumbai* - a 27 qubit device - and show that the accuracy of the measured observables is significantly improved after applying our Tensor Network compilation scheme.

1 Introduction

The simulation of quantum many-body systems is a task of immense scientific interest. The study of quantum dynamics, in particular, allows for the study of thermalisation, many-body localisation, Hubbard model physics and the applicability of field theory to out-of-equilibrium phenomena. In all of these fields there are many open scientific questions whose answers are likely to demand accurate simulation of quantum dynamics. However, the classical computational requirements of a brute-force approach to quantum dynamical simulations scales exponentially in the size of the system. Approximate techniques such as Tensor Networks are thus often called upon. Tensor Networks represent one of the best set of tools available to simulate time evolution and can also be applied to other problems such as ground state calculations [1] and machine learning [2, 3].

Matrix Product States (MPS) are a particular type of Tensor Network that are particularly suited to describe quantum systems in one dimension. They form a key component of modern implementations of the well known Density Matrix Renormalisation Group (DMRG) algorithm used to find the ground state of local Hamiltonians. The DMRG algorithm was designed many years before [4] it was realised that it could be understood as a variational optimisation algorithm where a Matrix Product State is used as an Ansatz for the ground state [5]. This insight shed light on the reasons behind the spectacular success of DMRG; the ground states of local Hamiltonians are only weakly entangled and so too are Matrix Product States. More precisely, the bipartite entanglement entropy S of the ground state of a local Hamiltonian satisfies an area law, meaning that the entanglement entropy is proportional to the area of the boundary of the two subsystems in the bipartition. In 1D, this means that the entanglement entropy is independent of the system size [6]. This is in contrast to typical states in Hilbert space whose entanglement structures satisfy a volume law. Matrix Product States are also known to satisfy an area law [5] and thus have the same entanglement structure as the ground state by design.

Since the weak entanglement of ground states of local Hamiltonians allow for their efficient storage as Matrix Product States, it is natural to ask if this is also possible for states that are generated by time evolution as these states are no longer necessarily weakly entangled. It turns out that for many physical systems of interest, entanglement entropy increases linearly until it saturates, at which point an MPS

will no longer be an efficient representation of the state. However, if the initial state is weakly entangled then the MPS representation can be used to store the state at early times. A paradigmatic example of this scenario is a quantum quench, whereby a quantum system is initially prepared in the ground state of some local Hamiltonian, the parameters of the Hamiltonian are subsequently changed very rapidly and the system then evolves according to Schrödinger's equation. The TEBD algorithm (Time Evolving Block Decimation) can be used to simulate time evolution after a quantum quench; the state is stored as an MPS and this MPS is updated as a function of time. Despite the success of DMRG, TEBD and other Tensor Network algorithms, these approaches are not without limitations. The memory requirements to store an MPS is characterised by the *bond dimension*, given by the dimension of the largest matrix used in the description of the state. For constant approximation error ϵ this bond dimension increases exponentially with the entanglement entropy and thus with time. Therefore, for a fixed maximum bond dimension, the error ϵ increases exponentially with time. This limits the applicability of Tensor Network algorithms to short time simulations. A quantum algorithm however, does not in principle suffer from this issue - the key difference between a quantum and a classical device being the ability to store highly entangled states. A quantum computer therefore has the potential to simulate quantum many-body systems for long times. The accurate simulation of the time evolution of 1D quantum systems is thus a promising route for the demonstration of quantum advantage in the short term. One such quantum algorithm is Trotterisation, where a discrete time step dt is used and the time evolution operator is approximated as a quantum circuit with an error that scales polynomially in dt . The depth of the quantum circuit used in such an approach increases with decreasing dt , leading to a trade-off between the noise arising from using deep circuits and the decreasing accuracy of the approximation when dt is increased. A number of variational quantum algorithms for the simulation of time evolution have therefore been developed that aim to use shallower circuits [7, 8, 9, 10]. Each of these approaches suffer from a number of issues such as convergence, runtime and limited device connectivity. As a result, it has been argued that such variational approaches are not practical for use on near term quantum hardware [11].

One approach that aims to overcome the issue of deep circuits is Approximate Quantum Compiling [12, 13, 14], where one defines a parametric circuit of fixed depth and uses techniques from optimisation to minimise the distance between the parametric circuit and the target circuit of interest - where distance is defined by some carefully chosen metric. In principle, this approach can lead to short depth circuits that implement the target circuit of interest within some error tolerance. In practice, a classical implementation of such an approach [14] is limited to act on a small number of qubits due to the exponential scaling of the Hilbert space with the number of qubits.

Here we develop a new approach to quantum simulation that combines Matrix Product States, Approximate Quantum Compiling and Trotterisation to produce short depth quantum circuits that implement the time evolution operator of the Heisenberg spin chain. This approach is scalable thanks to the immense power of Matrix Product States. Figure 1 shows a schematic of our approach: first we apply Trotterisation classically for the maximum length of time for which we can still store the state as an MPS. We then apply a Matrix Product State implementation of Approximate Quantum Compiling to squeeze the circuit (purple box in the figure) to find a much shallower circuit that still reproduces the same state as Trotterisation, up to some small error in the fidelity. We then use the squeezed circuit as the input for the Trotter circuit which can now generate a quantum state beyond what can be stored classically.

2 Setup

2.1 The model

We will consider the XXX spin-chain - a paradigmatic model for quantum magnetism - defined by the Hamiltonian:

$$H_{XXX} = - \sum_{i=0}^{L-1} h_{i,i+1} = - \sum_{i=0}^{L-1} (S_i^x S_{i+1}^x + S_i^y S_{i+1}^y + S_i^z S_{i+1}^z), \quad (1)$$

where S^x , S^y and S^z are written in terms of Pauli matrices as $S^x = \frac{\sigma^x}{2}$, $S^y = \frac{\sigma^y}{2}$ and $S^z = \frac{\sigma^z}{2}$. The Hamiltonian in (1) is a prototypical example of an integrable 1D model and its dynamical behaviour has been studied extensively [15], including on a quantum computer [16, 17]. The time evolution of a

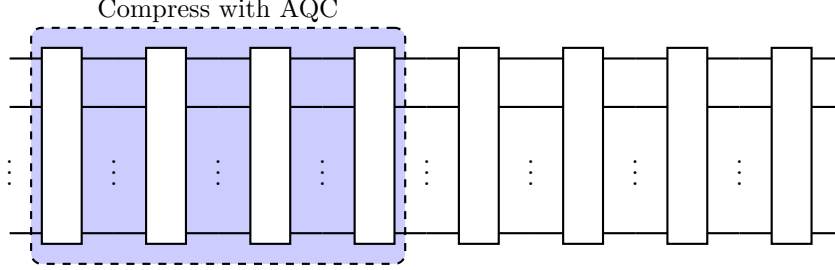


Figure 1: Schematic of our approach: Trotterisation is applied classically (purple box) and then a Matrix Product State implementation of Approximate Quantum Compiling is applied to compress the first part of the circuit. Standard Trotterisation is then applied on a quantum device afterwards to simulate longer times, i.e. times which are beyond what is possible classically.

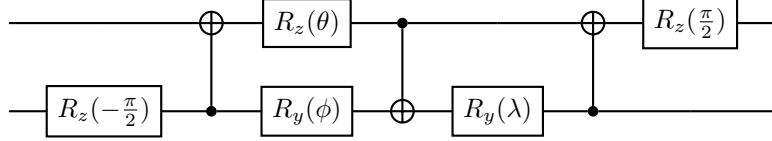


Figure 2: Implementation of two site operator $e^{i(\alpha\sigma^x\otimes\sigma^x + \beta\sigma^y\otimes\sigma^y + \gamma\sigma^z\otimes\sigma^z)}$ as a quantum circuit. We have the correspondences $\theta = \frac{\pi}{2} - 2\gamma$, $\phi = 2\alpha - \frac{\pi}{2}$ and $\lambda = \frac{\pi}{2} - 2\beta$. The Hamiltonian in (1) corresponds to the case $\alpha = \beta = \gamma = dt$

quantum state $|\psi(t)\rangle$ is governed by the Schrödinger equation:

$$|\psi(t)\rangle = e^{-iH_{XXX}t} |\psi(0)\rangle \quad (2)$$

where $|\psi(0)\rangle$ is the wavefunction at time $t = 0$. In this work, we will consider the Néel state, written as: $|\uparrow\downarrow\uparrow\dots\uparrow\downarrow\rangle$ where \uparrow and \downarrow represent up and down spins respectively. The Néel state for n spins is simply implemented on n qubits as $|1010\dots10\rangle$.

The time evolution operator $U(t) \equiv e^{-iHt}$ can be executed as a quantum circuit in a resource efficient way; we first write the Hamiltonian in (1) as $H_{XXX} = H_1 + H_2$ where $H_1 = -\sum_{i \text{ odd}} h_{i,i+1}$ and $H_2 = -\sum_{i \text{ even}} h_{i,i+1}$. Note that all operators in a given sum commute with all other operators in their respective sums. We then define the Suzuki-Trotter time evolution operator $\mathcal{U}_{\text{trot}}(dt)$ in the following way:

$$\mathcal{U}_{\text{trot}}^{(1)}(dt) = \prod_{j=0}^{L/2-1} U_{2j,2j+1}(dt) \prod_{j=1}^{L/2-1} U_{2j-1,2j}(dt) = e^{-iH_{XXX}dt} + O(dt^2) \quad (3)$$

where $U_{jk}(dt) = e^{-ih_{jk}dt}$. The exact time evolution operator $U(t)$ is thus approximated by m repeated applications of $\mathcal{U}_{\text{trot}}(dt = \frac{t}{m})$, i.e. $U(t) \approx \mathcal{U}_{\text{trot}}^m(dt = \frac{t}{m})$. As discussed in [17], each $U_{jk}(dt)$ appearing in (3) can be implemented by the quantum circuit with just three CNOTs as in Figure 2. We can reduce the error in the Trotter formula in equation (3) by using higher order expressions [18]. It turns out that the second order Trotter formula can be implemented on a quantum circuit with only one extra layer in the circuit [17]. We have:

$$\begin{aligned} \mathcal{U}_{\text{trot}}^{(2)}(dt) &= \prod_{j=0}^{L/2-1} U_{2j,2j+1}\left(\frac{dt}{2}\right) \prod_{j=1}^{L/2-1} U_{2j-1,2j}(dt) \prod_{j=0}^{L/2-1} U_{2j,2j+1}\left(\frac{dt}{2}\right) \\ &= e^{-iH_{XXX}dt} + O(dt^2) \end{aligned} \quad (4)$$

which can be implemented on a quantum device by the circuit in Figure 4.

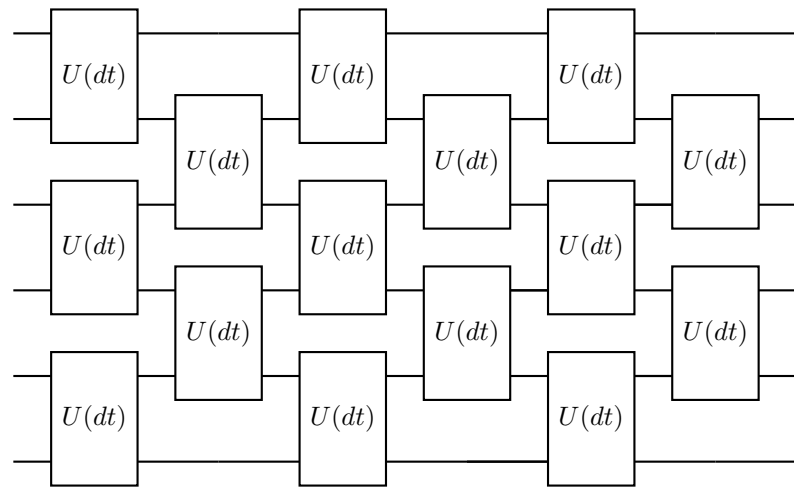


Figure 3: First order Trotter circuit acting on six qubits.

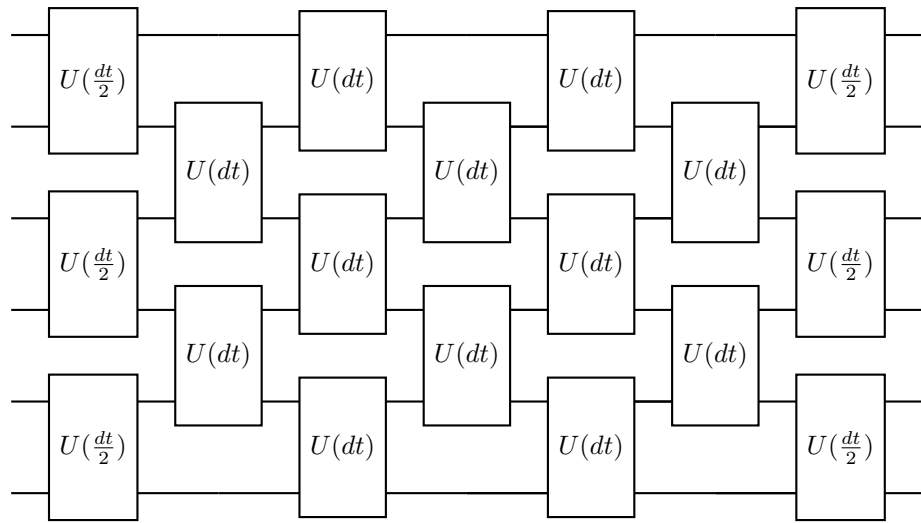


Figure 4: Second order Trotter circuit acting on six qubits.

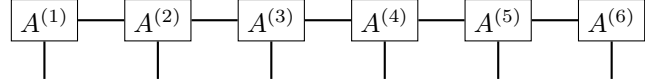


Figure 5: Graphical representation of an MPS. There are two matrices $A^{(i)}$ for each qubit at position i .

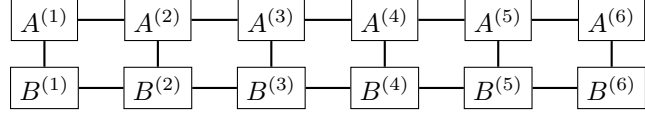


Figure 6: The inner product $\langle \psi_1 | \psi_2 \rangle$ of two Matrix Product States - see equations (11) and (6).

2.2 Matrix Product States

An arbitrary quantum state on n qubits can be written in terms of complex variables c_{j_1, \dots, j_n} , the number of which scales as 2^n :

$$|\psi\rangle = \sum_{\{j_1, \dots, j_n\}} c_{j_1, \dots, j_n} |j_1, \dots, j_n\rangle \quad (5)$$

where the sum is over all configurations of the binary variables j_1, \dots, j_n . The bipartite entanglement entropy of an arbitrary quantum state picked at random from Hilbert space satisfies a volume law which, as was discussed in the introduction, is distinct from area law entanglement in which case the entanglement entropy of two regions after the bipartition of the system is proportional to the area of the boundary of the system. A small subset of states in Hilbert space satisfies an area law. The coefficients c_{j_1, \dots, j_n} of such states have a certain structure that we can take advantage of to study classically. Any state $|\psi\rangle$ can be written in the following way:

$$c_{j_1, \dots, j_n} = A_{j_1}^{(1)} \cdot A_{j_2}^{(2)} \cdots \cdot A_{j_n}^{(n)} \quad (6)$$

where the A_j are $\chi_j \times \chi_{j+1}$ dimensional matrices. Quantum states of the form (6) are known as Matrix Product States (MPS). The maximum value of χ_j is referred to as the bond dimension of the MPS. We can represent an MPS graphically as in Figure 5. We associate one matrix $A^{(i)}$ to each qubit. Note that for each qubit i we have two matrices. We thus have a total of $2n$ matrices to keep track of. The bond dimension χ_j can be seen as a measure of the entanglement between the two subsystems when a bipartition is made at qubit j . Therefore, states in Hilbert space that satisfy an area law - and therefore have a low bond dimension in their MPS representation - can be efficiently stored as Matrix Product States. States that satisfy a volume law will have a bond dimension that is exponential in the number of qubits. We will consider in this work the non-trivial dynamics governed by equation (2). As discussed in the introduction, the bipartite entanglement entropy of a ground state of a one-dimensional Hamiltonian that has a gap between its ground state and its excited state is independent of the size of the subsystems. The ground state of such a system - and hence the initial state in our setup - can be efficiently stored as an MPS. One can then use an algorithm such as TEBD (Time Evolving Block Decimation) [19] to update the MPS as a function of time to study the dynamics of the system. However, the entanglement entropy of the state increases linearly with time, hence the bond dimension χ that is required to keep the error constant diverges exponentially with time. To simulate for longer times, a quantum computer would be needed. In section 2.3, we will discuss how Matrix Product States can be leveraged to reduce the resource requirements for this simulation problem when implemented on a quantum device.

2.3 Matrix Product States applied to Approximate Quantum Compiling

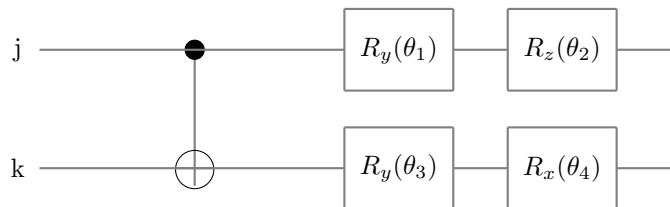


Figure 7: *CNOT* block forms the basic building block of our circuit ansatz.

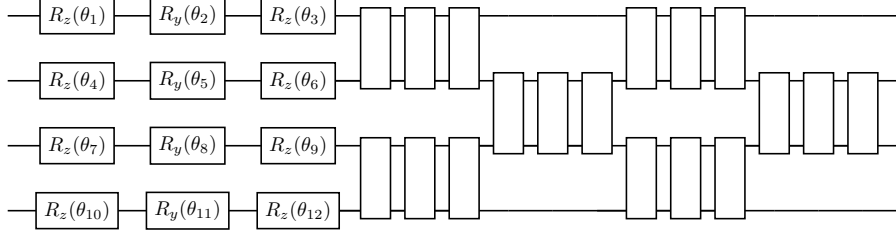


Figure 8: Parameterised circuit inspired by the structure of the first order Trotter circuit in Figure 3.

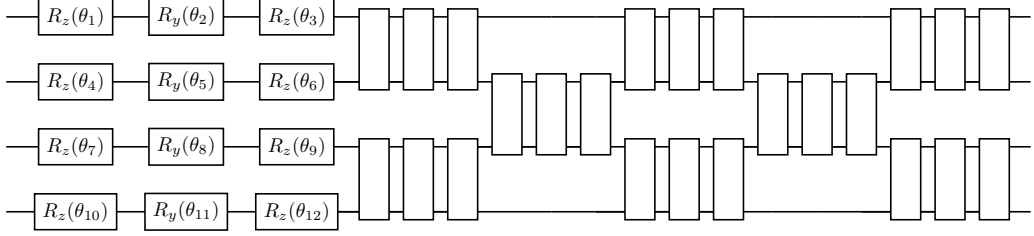


Figure 9: Parameterised circuit inspired by the structure of the second order Trotter circuit in Figure 4.

Approximate quantum compiling (AQC) involves the design of a parametric quantum circuit with fixed depth - the parameters are then adjusted to bring it as close as possible to the target, where “close” is defined via some carefully chosen metric, see below. As discussed in [12], one can use so-called *CNOT* blocks to construct a natural circuit Ansatz. A *CNOT* block is a *CNOT* gate followed by single qubit rotations (see Figure 7). A block with a *CNOT* gate acting on a “control” qubit j and “target” qubit k is written as $\text{CU}_{jk}(\theta_1, \theta_2, \theta_3, \theta_4)$. For a given hardware connectivity, one can then write down a fully parameterised circuit as:

$$V_{\text{ct}}(\boldsymbol{\theta}) = \text{CU}_{\text{ct}(L)}(\theta_{3n+4L-3}, \dots, \theta_{3n+4L}) \cdots \text{CU}_{\text{ct}(1)}(\theta_{3n+1}, \dots, \theta_{3n+4}) \quad (7)$$

$$[R_z(\theta_1) R_y(\theta_2) R_z(\theta_3)] \otimes \cdots \otimes [R_z(\theta_{3n-2}) R_y(\theta_{3n-1}) R_z(\theta_{3n})]$$

The position of the *CNOT* blocks in the parameterised circuit can be customised to suit the particular target circuit that one is interested in. Here we are interested in finding a circuit that implements the unitary time evolution operator as in equation (2). We thus consider a structure inspired by the first and second-order Trotter circuits in Figures 3 and 4 respectively. Recall that each block $U(dt)$ in Figures 3 and 4 represents the 2-qubit sub-circuit with three *CNOT*s in Figure 2; it is therefore natural to consider a circuit Ansatz with sub-circuits each with three *CNOT* blocks as in Figures 8 and 9, such that the circuit Ansatz mimics the structure of the first and second order Trotter circuits. In the notation of [14], the parameterised circuits in Figures 8 and 9 correspond to $n = 4$ qubits, $l = 2$ layers and $b = 3$ *CNOT* blocks in each layer. In both Figure 8 and Figure 9 there are three rotation gates acting on each qubit at the beginning of the circuit. In the examples considered in this work we will take the initial state to be $|0\rangle$ - the initial rotation gate $R_z(\theta)$ is redundant for these cases but is necessary for more general initial states.

One can define the distance between the target and parameterised circuit via a number of different metrics. Here we use a cost function based on the Hilbert-Schmidt test:

$$C_{hs}^{\text{state}} = 1 - |\langle 0 | V^\dagger(\boldsymbol{\theta}) | \psi_0 \rangle|^2 \quad (8)$$

The goal of AQC is to tune the parameters $\boldsymbol{\theta}$ to minimise the cost function under consideration. Note that here we are considering the application of AQC to state preparation as opposed to full circuit compilation. More precisely, this means that our cost function is designed such that it is minimised when the action of $V(\boldsymbol{\theta})$ on the initial state $|0\rangle$ produces a state that is as close as possible to a target state $|\psi_0\rangle$ (up to some global phase). This is in contrast to the situation where one starts with some target *circuit* U and the cost function is designed to bring the full matrix $V(\boldsymbol{\theta})$ as close as possible to U .

As pointed out in [20], the gradient of the cost function in (8) vanishes exponentially. This observation lead to the distinction between global and local cost functions; local cost functions have only polynomially vanishing gradients in some cases of interest - see [20, 21, 14] for details. As was shown in [14], the Hilbert-Schmidt test - which is a global cost function - can be turned into a local one by adding several “bit-flip” terms which increases the magnitude of the gradient:

$$\begin{aligned} C_{lhs}^{\text{state}} = 1 - & |\langle 0 | V^\dagger(\theta) | \psi_0 \rangle|^2 - \left(\frac{n-1}{n} \right) \sum_{j=1}^n |\langle 0 | X_j V^\dagger(\theta) | \psi_0 \rangle|^2 \\ & - \left(\frac{n-2}{n} \right) \sum_{j < k} |\langle 0 | X_j X_k V^\dagger(\theta) | \psi_0 \rangle|^2 - \dots - \frac{1}{n} \sum_{j < k < l < \dots} |\langle 0 | X_j X_k X_l \dots V^\dagger(\theta) | \psi_0 \rangle|^2 \end{aligned} \quad (9)$$

Convergence of the cost function can be significantly improved by adding these terms, however the computational cost of calculating the gradient becomes prohibitive. It was demonstrated in [14] that this can be overcome by truncating the expression in (9) to get:

$$C_L^{(1)}(\alpha) = 1 - |\langle 0 | V^\dagger(\theta) | \psi_0 \rangle|^2 - \alpha \sum_{j=1}^n |\langle 0 | X_j V^\dagger(\theta) | \psi_0 \rangle|^2 \quad (10)$$

where α is a parameter that can be tuned throughout the optimisation procedure - a scheme to implement this tuning effectively was demonstrated in [14]. In (10), we have only kept 1 “bit-flip” term, i.e. we have dropped all terms with more than one *NOT* operators X_i . As discussed in [14], one can obtain higher order expressions $C_L^{(k)}$ with more “bit-flip” terms included - doing so induces a larger gradient in the cost function but increases the computational burden.

Note that each term in (9) or (10) is an overlap of quantum states, and since the overlap of two MPS can be calculated very efficiently the architecture of Matrix Product States can be leveraged to calculate the cost function and solve the approximate quantum compilation problem for large numbers of qubits. Consider for example two quantum states $|\psi_1\rangle$ and $|\psi_2\rangle$:

$$\begin{aligned} |\psi_1\rangle &= \sum_{\{j_1, \dots, j_n\}} c_{j_1, \dots, j_n}^{(1)} |j_1, \dots, j_n\rangle \\ |\psi_2\rangle &= \sum_{\{j_1, \dots, j_n\}} c_{j_1, \dots, j_n}^{(2)} |j_1, \dots, j_n\rangle \end{aligned} \quad (11)$$

As discussed in section 2.2, for weakly entangled states the coefficients $c_{j_1, \dots, j_n}^{(1)}$ and $c_{j_1, \dots, j_n}^{(2)}$ are not all independent and can be represented efficiently as Matrix Product States - see Figure 5:

$$\begin{aligned} c_{j_1, \dots, j_n}^{(1)} &= A_{j_1}^{(1)} \cdot A_{j_2}^{(2)} \cdots \cdot A_{j_n}^{(n)} \\ c_{j_1, \dots, j_n}^{(2)} &= B_{j_1}^{(1)} \cdot B_{j_2}^{(2)} \cdots \cdot B_{j_n}^{(n)} \end{aligned} \quad (12)$$

We want to calculate the quantity:

$$f(|\psi_1\rangle, |\psi_2\rangle) = |\langle \psi_1 | \psi_2 \rangle|^2 \quad (13)$$

The overlap of two MPS, and hence the fidelity f in (13) can be calculated efficiently by “contracting” the Tensor Network shown in Figure 6.

3 Results

We now present the results of our simulations of the Schrödinger equation in equation (2) using the second order Trotter formula in equation (4). First let’s define and clarify some notation:

- $|a_1\rangle$: The state generated by the optimised parametric circuit in Figure 9.
- Number of layers l in Ansatz: in Figures 8 and 9 there are $l = 2$ layers.
- $|t_1\rangle$: The state generated by the Trotter circuit in Figure 4.

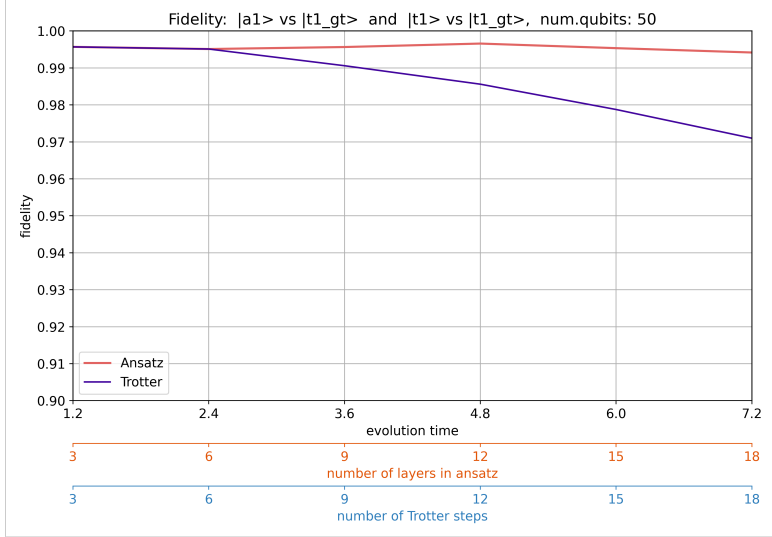


Figure 10: 50 qubits: fidelities of the parametric circuit and the Trotter circuit with the "ground truth" obtained by Tensor Network simulations. The two circuits are of identical length but the parametric circuit achieves a significantly higher fidelity at late times.

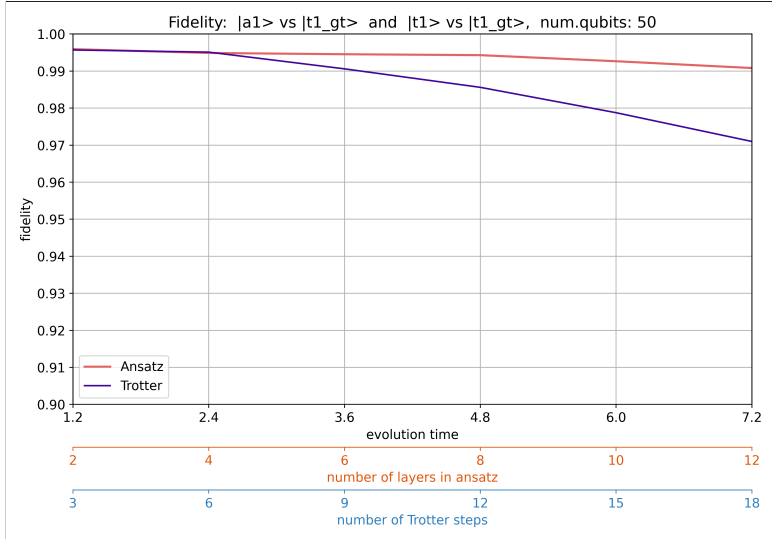


Figure 11: 50 qubits: the maximum number of layers in the parametric circuit is 12 while it is 18 for the Trotter circuit. Despite this, the parametric circuit achieves a higher fidelity.

- Number of Trotter steps: the analogue of the number of layers in the Ansatz circuits. In Figure 3 and 4 there are 3 Trotter steps.
- $|t1_gt\rangle$: the "ground truth" generated by classical Tensor Network simulations of deep Trotter circuits, i.e. extremely small time steps. We take $dt = 0.04$ to generate the ground truth state while $|t_1\rangle$ is generated with a time step of $dt = 0.4$.

All circuits considered here take the form of the second-order Trotter structure. More precisely, in each graph we use the labels "Trotter" and "Ansatz" and these circuits have the structure in Figures 4 and 9 respectively. In Figures 10, 11 and 12 we plot fidelity vs evolution time for the 50 qubit XXX Hamiltonian and we compare the result of the Trotter circuit vs the AQC circuit. In Figure 10 we can see that the fidelity of the Trotter circuit decays rapidly while the fidelity of the AQC circuit remains above 0.99. Note that the Trotter circuit and the AQC circuit are of equal depth. In Figures 11 and 12 we compare short depth circuits generated by AQC with deep Trotter circuits. We observe that the AQC circuits can achieve comparable or better fidelities with much shorter depth. In particular, in Figure 12 the two fidelities are almost identical but the AQC circuit is half the depth of the Trotter circuit. We plot the

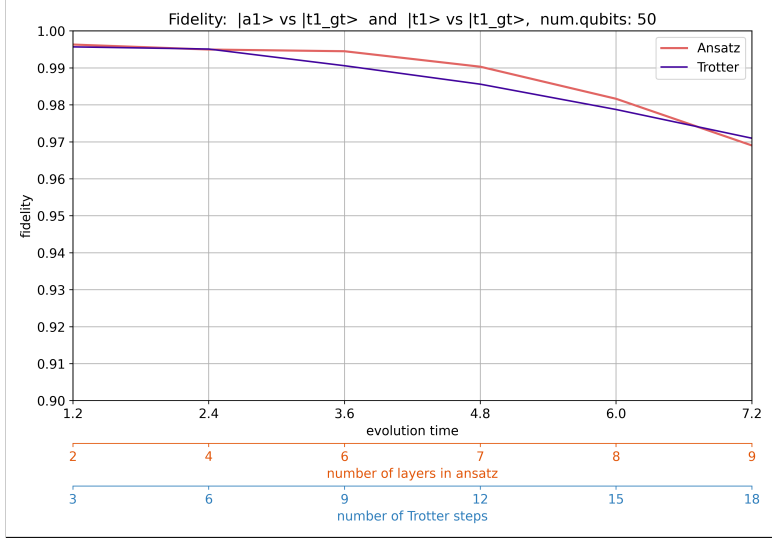


Figure 12: 50 qubits: the maximum number of layers in the parametric circuit is 9 while it is 18 for the Trotter circuit. Both circuits achieve very similar fidelities despite the parametric circuit being half the depth of the Trotter circuit.

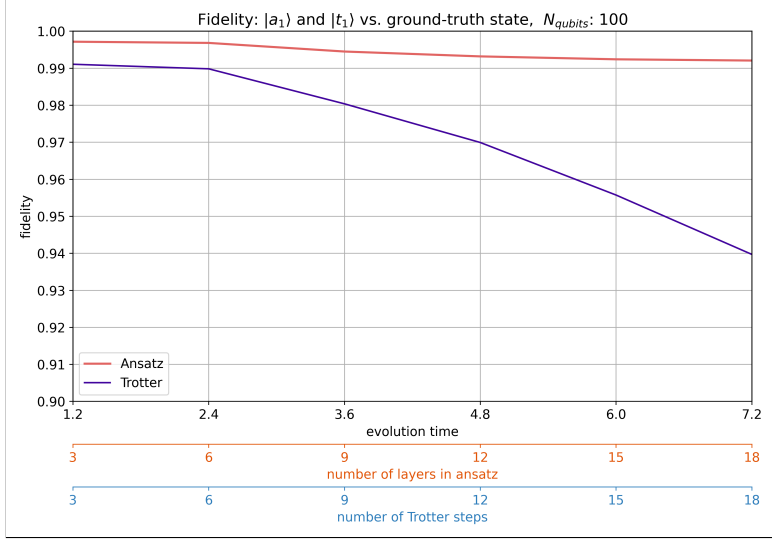


Figure 13: 100 qubits: The maximum number of layers in the parametric circuit and the Trotter circuit is 18. It can be seen that the fidelity of the Trotter circuit decays rapidly but that of the parametric circuit remains high.

same data for 100 qubits in Figures 13 and 14.

Now we would like to consider how these results affect the implementation on a real quantum device. We consider a 20 qubit spin-chain on the 27 qubit device *ibmq-mumbai*. First we plot the fidelity results for 20 qubits in Figure 15. We ran the resulting parametric circuit on *ibmq-mumbai* and in Figure 16 we plot the expectation values $\langle \psi(t) | S_0^z | \psi(t) \rangle$ as obtained from the quantum device using the parametric AQC circuit, the Trotter circuit and from a classical Tensor Network simulation. We observe that this observable is more accurate when obtained with the AQC circuit due to its reduced depth. Note that the difference between the results from the simulation and the results from the quantum device would be greatly reduced after applying error mitigation [22, 23]. We have not attempted to apply error mitigation to either circuit as this would be outside the scope of this work. We expect that, since our Tensor Network compilation scheme greatly reduces the noise of the circuit, any error mitigation scheme would be enhanced by our approach.

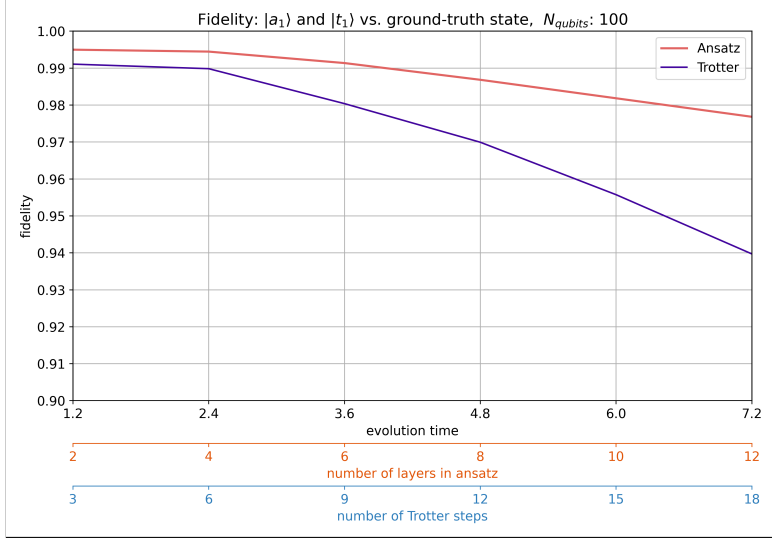


Figure 14: 100 qubits: The maximum number of layers in the parametric circuit is 12 while it is 18 for the Trotter circuit.

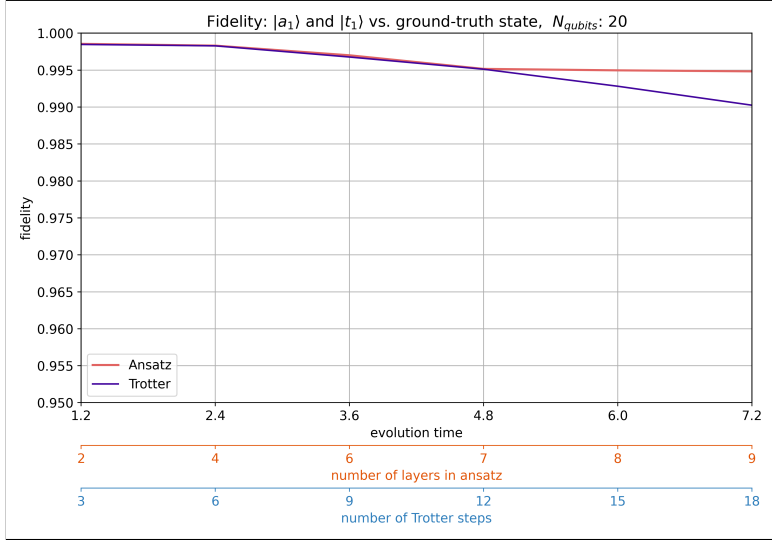


Figure 15: The maximum depth of the parametric circuit is half that of the Trotter circuit - there are 9 and 18 layers respectively. These 20 qubit circuits were implemented on *ibmq-mumbai* - see Figure 16.

4 Discussion

In this paper we applied Tensor Network methods to Quantum Compiling and demonstrated their efficacy on the 27 qubit device *ibmq-mumbai*. Our method is similar in spirit to [24] where Matrix Product States were used to prepare the initial state for VQE to find the ground state of some Hamiltonian - here we use Matrix Product States to prepare a short depth quantum circuit that simulates the time evolution of a 1D Hamiltonian. We chose the XXX Hamiltonian in equation (1) because it has been well studied, but we would be particularly interested to apply the compilation methods developed here to non-integrable systems by e.g. adding a random field to the Hamiltonian in (1) and studying phenomena of scientific interest such as many-body localisation.

We have shown results of our simulations on up to 100 qubits. In principle we can significantly increase the number of qubits and the length of time to which we apply our MPS compilation scheme; the limiting factor at present seems to be the particular implementation that we apply to SVD and to calculate the gradient. We believe that both of these can be improved significantly, in particular by using an efficient parallel implementation - this is the subject of ongoing work. In our current framework we use the Qiskit

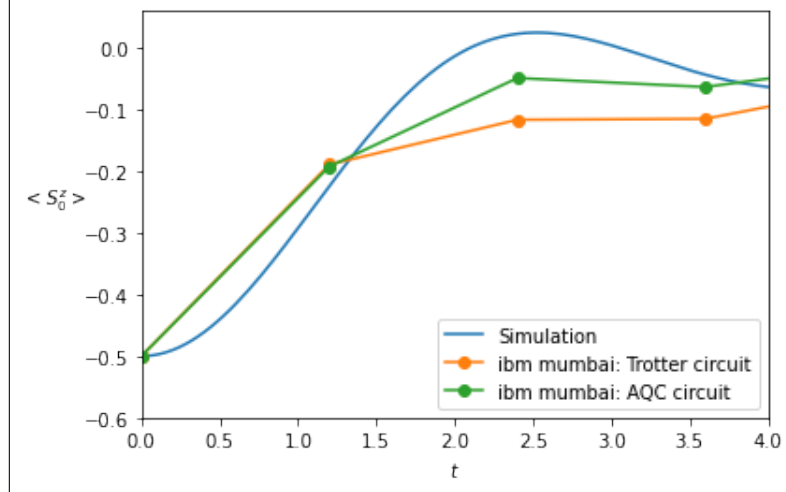


Figure 16: The expectation value of S_0^z vs time for a chain of 20 qubits as measured on the 27 qubit quantum device *ibmq-mumbai*. The circuit produced from our MPS implementation of AQC uses is shallower than the Trotter circuit, and thus produces an expectation value that is much closer to the true value plotted in the blue curve, obtained by classical Tensor Network simulations.

MPS package which is designed for generic situations in which long range connectivity may be required and thus does not take advantage of the short range structure of the circuits in Figures 8 and 9.

5 Acknowledgements

This work was funded by the Disruptive Technologies Innovation Fund (DTIF), by Enterprise Ireland, under project number DTIF2019-090 (project QCoIR) and also supported by IBM Quantum.

References

- [1] Frank Verstraete and J Ignacio Cirac. Matrix product states represent ground states faithfully. *Physical review b*, 73(9):094423, 2006.
- [2] Edwin Stoudenmire and David J Schwab. Supervised learning with tensor networks. *Advances in Neural Information Processing Systems*, 29, 2016.
- [3] Tom Vieijra, Laurens Vanderstraeten, and Frank Verstraete. Generative modeling with projected entangled-pair states. *arXiv preprint arXiv:2202.08177*, 2022.
- [4] Steven R White. Density-matrix algorithms for quantum renormalization groups. *Physical review b*, 48(14):10345, 1993.
- [5] Ulrich Schollwöck. The density-matrix renormalization group in the age of matrix product states. *Annals of physics*, 326(1):96–192, 2011.
- [6] Matthew B Hastings. An area law for one-dimensional quantum systems. *Journal of statistical mechanics: theory and experiment*, 2007(08):P08024, 2007.
- [7] Joe Gibbs, Kaitlin Gili, Zoë Holmes, Benjamin Commeau, Andrew Arrasmith, Lukasz Cincio, Patrick J Coles, and Andrew Sornborger. Long-time simulations with high fidelity on quantum hardware. *arXiv preprint arXiv:2102.04313*, 2021.
- [8] Cristina Cirstoiu, Zoe Holmes, Joseph Iosue, Lukasz Cincio, Patrick J Coles, and Andrew Sornborger. Variational fast forwarding for quantum simulation beyond the coherence time. *npj Quantum Information*, 6(1):1–10, 2020.
- [9] Christa Zoufal, David Sutter, and Stefan Woerner. Error bounds for variational quantum time evolution. *arXiv preprint arXiv:2108.00022*, 2021.
- [10] Kishor Bharti and Tobias Haug. Quantum-assisted simulator. *Physical Review A*, 104(4):042418, 2021.
- [11] Alexander Miessen, Pauline J Ollitrault, and Ivano Tavernelli. Quantum algorithms for quantum dynamics: a performance study on the spin-boson model. *Physical Review Research*, 3(4):043212, 2021.
- [12] Liam Madden and Andrea Simonetto. Best approximate quantum compiling problems. *ACM Transactions on Quantum Computing*, 3(2):1–29, 2022.
- [13] Liam Madden, Albert Akhriev, and Andrea Simonetto. Sketching the best approximate quantum compiling problem. *arXiv preprint arXiv:2205.04025*, 2022.
- [14] Niall F Robertson, Albert Akhriev, Jiri Vala, and Sergiy Zhuk. Escaping barren plateaus in approximate quantum compiling. *arXiv preprint arXiv:2210.09191*, 2022.
- [15] Lorenzo Piroli, Balázs Pozsgay, and Eric Vernier. From the quantum transfer matrix to the quench action: the loschmidt echo in xxz heisenberg spin chains. *Journal of Statistical Mechanics: Theory and Experiment*, 2017(2):023106, 2017.
- [16] Nathan Keenan, Niall Robertson, Tara Murphy, Sergiy Zhuk, and John Goold. Evidence of kardar-parisi-zhang scaling on a digital quantum simulator. *arXiv preprint arXiv:2208.12243*, 2022.
- [17] Adam Smith, MS Kim, Frank Pollmann, and Johannes Knolle. Simulating quantum many-body dynamics on a current digital quantum computer. *npj Quantum Information*, 5(1):1–13, 2019.
- [18] David Layden. First-order trotter error from a second-order perspective. *Physical Review Letters*, 128(21):210501, 2022.
- [19] Johannes Hauschild and Frank Pollmann. Efficient numerical simulations with tensor networks: Tensor network python (tenpy). *SciPost Physics Lecture Notes*, page 005, 2018.
- [20] Sumeet Khatri, Ryan LaRose, Alexander Poremba, Lukasz Cincio, Andrew T Sornborger, and Patrick J Coles. Quantum-assisted quantum compiling. *Quantum*, 3:140, 2019.

- [21] Marco Cerezo, Akira Sone, Tyler Volkoff, Lukasz Cincio, and Patrick J Coles. Cost function dependent barren plateaus in shallow parametrized quantum circuits. *Nature communications*, 12(1):1–12, 2021.
- [22] Kristan Temme, Sergey Bravyi, and Jay M Gambetta. Error mitigation for short-depth quantum circuits. *Physical review letters*, 119(18):180509, 2017.
- [23] Youngseok Kim, Christopher J Wood, Theodore J Yoder, Seth T Merkel, Jay M Gambetta, Kristan Temme, and Abhinav Kandala. Scalable error mitigation for noisy quantum circuits produces competitive expectation values. *arXiv preprint arXiv:2108.09197*, 2021.
- [24] Manuel S Rudolph, Jacob Miller, Jing Chen, Atithi Acharya, and Alejandro Perdomo-Ortiz. Synergy between quantum circuits and tensor networks: Short-cutting the race to practical quantum advantage. *arXiv preprint arXiv:2208.13673*, 2022.